Lamb wave attenuation in a rough plate. II. Analytical and numerical results in a fluid plate

Catherine Potel,[1,4,a)] Damien Leduc,[2,4] Bruno Morvan,[2,4] Claude Depollier,[1,4] Anne-Christine Hladky-Hennion,[3,4] Jean-Louis Izbicki,[2,4] Pascal Pareige,[2,4] and Michel Bruneau[1,4]

[1]*Laboratoire d'Acoustique de l'Université du Maine (LAUM), UMR CNRS 6613, 72085, Le Mans, France*
[2]*Laboratoire d'Ondes et Milieux Complexes (LOMC) FRE CNRS 3112, Université du Havre, 76600 Le Havre-France*
[3]*Institut d'Electronique, de Microélectronique et de Nanotechnologie (IEMN), UMR CNRS 8520, 59046 Lille, France*
[4]*Fédération Acoustique du Nord-Ouest, (FANO), FR CNRS 3110, France*

(Received 12 February 2008; accepted 20 July 2008; published online 3 October 2008)

This paper aims at providing analytical and numerical approaches to analyze the behavior of guided waves (Lamb-type waves) propagating inside plates with a rough surface considered here as distributed small perturbations. A physical interpretation of the attenuation phenomenon of the propagating mode generated by the source (mode coupling) is provided for an ideal rough plate (fluid plate) using an analytical model available in the literature. This analytical model is validated using a numerical method. The obtained results on periodically corrugated surfaces of fluid plates emphasize the role played by the spatial period and the modal coupling. They serve also as results for interpreting the effect due to randomly rough surfaces in solid plates, notably the effect of the power spectrum density of the rough profile (including the effect of the statistical roughness parameters mentioned in Part I). The results obtained experimentally and theoretically, for the attenuation factor of the main Lamb wave, are found close to one another. © *2008 American Institute of Physics*. [DOI: 10.1063/1.2979851]

I. INTRODUCTION

The characterization of bounded roughened surfaces before applying adhesive joint, in order to detect poor cohesive and adhesive properties, remains difficult. Earlier studies based on the analysis of surface waves (Rayleigh waves or Scholte waves) are not really adapted for the characterization of such surfaces (see Refs. 1–13 and references contained therein). Guided acoustic waves, i.e., Lamb waves, turn out to be the best adapted kind of waves to characterize this roughness when plates are bounded together.

In a previous work,[14] analytic solutions for describing the acoustic coupling in fluid-filled rough waveguides were given. This model involves the use of Green's theorem and perturbation method in the frame of a modal analysis. The roughness is described exactly by the depth and the slope of the profile; the wavelength is assumed to be much greater than the depth of the roughness profile. With a view, as in Part I (companion paper[13]), of characterizing bounded roughened surfaces before applying an adhesive joint in order to detect poor cohesive and adhesive properties, this paper aims at providing the results obtained both from the above-mentioned analytical model[14] and from a numerical model [finite element method (FEM)]. It deals with the propagation of guided, longitudinal acoustic waves in a planar waveguide having rough surfaces. A physical interpretation of several phenomena involved in the presence of roughness is given: it emphasizes first modal coupling in the rough boundary and second phonon relationships, which are related to the incident wave, the converted modes, and the grating.[15–17] Notably, the paper deals with (i) an analytical estimation of the attenuation factor of the guided wave (in good agreement with the experimental results[9]) and (ii) a numerical validation of the analytical model using FEM.

II. INTEREST OF THE FLUID PLATE REGARDING THE SOLID PLATE

The three-dimensional model developed in Ref. 9 for an anisotropic rough plate is a shape profile model with a monomode approach: the scattering of a main Lamb mode on the shape perturbation of the boundaries is taken into account, which leads to a dispersion equation of the form

$$F(k_1,\omega) \approx F_0(k_1,\omega) + \delta F(k_1,\omega) = 0, \tag{1}$$

where the function $F_0(k_1,\omega)$ corresponds to the dispersion equation for classical Lamb modes in a plate with plane surfaces and $\delta F(k_1,\omega)$ is a perturbation term. For a given angular frequency ω, the solution k_1 of the dispersion in Eq. (1) can be written as (its real and imaginary parts denoted k_1' and k_1'', being related, respectively, to the shift frequency and to the attenuation of the wave)

$$k_1 = k_{1_0} + \delta k_1, \tag{2}$$

with the roughness of the stress-free boundary inducing a small complex perturbation $\delta k_1 = \delta k_1' + i\,\delta k_1''$.

Therefore, the consequences of the scattering of the main Lamb mode on the roughness (especially the imaginary

a)Author to whom correspondence should be addressed: Tel.: 33 2 43 83 36 17. FAX: 33 2 43 83 35 20. Electronic mail: catherine.potel@univ-lemans.fr.

TABLE I. Characteristics of the fictitious fluid (glass with only longitudinal waves) and characteristics of the roughness as the function of the dimensionless parameters fd/c_0 and d/Λ: $k_0=(2\pi/d)(fd/c_0)$; $\lambda=d/(fd/c_0)$; $f=(c_0/d)(fd/c_0)$; $\Lambda/\lambda=(fd/c_0)/(d/\Lambda)$; $\ell=(2N-1)\Lambda/2$.

			"Glass" (for longitudinal waves)
		c_0 (m s^{-1})	5825
		ρ (kg m^{-3})	5000
		d (m)	0.005
$fd/c_0=0.92$		λ (m)	0.0054
$d/\Lambda=5/3$		Λ/λ	0.555
		f (MHz)	1.0718
		k_0(m^{-1})	1156
	$k_0\ell=450$; $N=130$	ℓ(m)	0.388
$fd/c_0=0.91$		λ (m)	0.0055
$d/\Lambda=5/3$		Λ/λ	0.55
		f (MHz)	1.06
		k_0 (m^{-1})	1143
	$k_0\ell=37.7$; $N=11$	ℓ(m)	0.033

part k_1'' of the wavenumber k_1 related to the attenuation) are observed on a main Lamb mode. Actually, the complex perturbation δk_1 of the wavenumber k_{1_0}, which is associated with the main Lamb mode without roughness [see Eq. (2)], corresponds to a loss of energy in the main Lamb mode through energy transfers between modes, but these phenomena have not been described in the analytical procedure. The results obtained (Ref. 13, Sec. IV) show mainly that the spatial period Λ involved in the rough profile (through the power spectrum density of the profile) is an important parameter.

In order to better understand the involved phenomena, the behavior of a much simpler medium (a fictitious fluid plate—the properties of which are close to those of glass, see Table I) is modeled, taking into account all the modes, which could be created by the scattering of a main Lamb mode on the roughness. This is an intermodal approach.

The theoretical model and its main results[14] are summarized in Sec. III, showing more particularly the influence of the spatial period Λ on the amplitude of the modes and providing an understanding of these basic physical phenomena. A comparison with the results obtained by FEM approach is then presented in Sec. IV.

III. SHAPE PROFILE MODEL FOR A FLUID ROUGH PLATE: INTERMODAL APPROACH, PHONON RELATIONSHIP

This section is based on Ref. 14 (most of the theoretical relations are given with more details in this reference). The waveguide is assumed to be limited by two parallel rigid plates having two-dimensional shape perturbations (three-dimensional problem). The fluid plate (speed of sound c_0), with regularly shaped surfaces $x_3=0$ and $x_3=\delta$, which encloses the real waveguide, is characterized by its thickness δ. The inner plate surrounded by the real waveguide is characterized by its thickness d (see Fig. 1). The depths of the small shape deviations are, respectively, denoted $H_0(x_1,x_2)$ and $H_d(x_1,x_2)$ at $x_3=0$ and $x_3=\delta$.

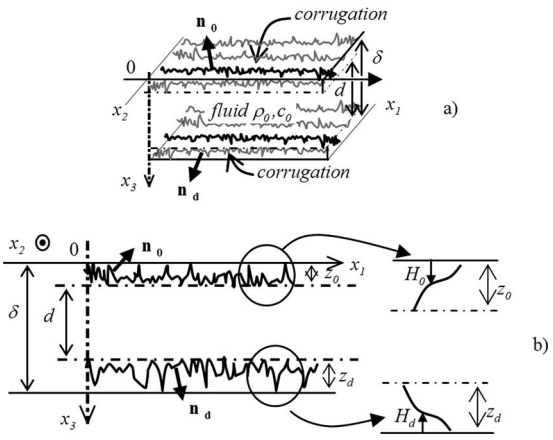

FIG. 1. Fluid plate between two perturbed boundary surfaces.

The acoustic pressure field $\hat{P}(x_1,x_2,x_3;\omega)$ in the perturbed plate is expressed as an eigenfunction expansion, the orthogonal eigenfunction $\psi_m(x_3)$ being the solution of the Neumann boundary problem in the regularly shaped waveguide for which surfaces bound the perturbed waveguide [see Eqs. (8) and (9) in Ref. 14],

$$\hat{p}(x_1,x_2,x_3;t)=\hat{P}(x_1,x_2,x_3;\omega)e^{i\omega t}=\sum_m \hat{A}_m(x_1,x_2)\psi_m(x_3)e^{i\omega t}, \tag{3}$$

where

$$\psi_m(x_3)=\sqrt{(2-\delta_{m0})/\delta}\cos(k_m x_3), \tag{4a}$$

with

$$k_m=m\pi/\delta, \quad m\in\mathbb{N}. \tag{4b}$$

The coefficients $\hat{A}_m(x_1,x_2)$ are determined using methods relying on integral formulation and modal analysis and using the appropriate Green function $G_m(x_1,x_2;x_1',x_2')$.[18] The solution is obtained from an iterative method to express the amplitude of each mode $\hat{A}_m(x_1,x_2)$, the lower order (Born approximation) $\hat{A}_m^{(0)}$ being given by

$$\hat{A}_m^{(0)}(x_1,x_2)=\hat{Q}_m G_m(x_1,x_2;0,0), \tag{5}$$

where $\hat{Q}_m$ is the strength of a monochromatic source (which is assumed to be flush-mounted at $x_1=0$ and $x_2=0$) related to the mth mode. In fact, it represents the energy transfer between the external source and the eigenmode m. The first-order perturbation expansion

$$\hat{A}_m^{[1]}=\hat{A}_m^{(0)}+\hat{A}_m^{(1)} \tag{6}$$

is then obtained from [see Eq. (43) in Ref. 14]

$$\hat{A}_m^{(1)}(x_1,x_2)=\sum_\mu \hat{Q}_\mu \int_{-\infty}^{+\infty}\int_{-\infty}^{+\infty} G_m(x_1,x_2;x_1',x_2')\hat{\gamma}_{\mu m}(x_1',x_2') \times G_\mu(x_1',x_2';0,0)dx_1'dx_2' + \sum_{\mu\neq m}\hat{Q}_{\mu_1}(k_{x_1 m}^2-k_{x_1\mu}^2)\int_{-\infty}^{+\infty}\int_{-\infty}^{+\infty}$$

$$\times G_m(x_1,x_2;x_1',x_2')N_{\mu m}(x_1',x_2')G_\mu(x_1',x_2';0,0)$$
$$\times dx_1'dx_2', \tag{7}$$

where

$$k_{x_1 m}^2 = k_0^2 - k_m^2 \quad \text{with} \quad k_0 = \omega/c_0, \tag{8}$$

$$N_{\mu m}(x_1,x_2) = \int_{H_0}^{\delta - H_d} \psi_m(x_3)\psi_\mu(x_3)dx_3 \tag{9}$$

and where the coupling factor $\hat{\gamma}_{\mu m}(x_1',x_2')$ is a derivative operator (with respect to x_1' and x_2') acting on the Green function $G_\mu(x_1',x_2';0,0)$. This operator, $\hat{\gamma}_{\mu m}(x_1',x_2')$, involves the partial derivatives of the rough profiles $H_0(x_1',x_2')$ and $H_d(x_1',x_2')$ with respect to x_1' and to x_1' (it is related to the coupling through the slope and the depth of the surface perturbation itself). The general expression of the higher orders is given in Ref. 14, Sec. IV.

The summations over modes μ in Eq. (7) are representative of the intermodal couplings between the mode m generated by the source and all the modes (denoted μ) created by the scattering on the roughness. The integrals from $(-\infty)$ to $(+\infty)$ indicate that the coupling source is the roughness (which is an extended source); they represent the nonlocal effects of the roughness. In other words, these integrals and the use of the Green function $G_m(x_1,x_2;x_1',x_2')$ emphasize that the roughness before and after the measurement point (x_1,x_2) does not act on the coupling in the same way. Moreover, as these integrals involve the rough profile, they are related to the Power Spectrum Density (PSD) of the rough profile, and thus to the spatial periods Λ (see Ref. 13, Secs. II B and IV B).

As far as these spatial periods are concerned, for a periodic roughness of spatial period Λ, the relationships between both the length of the spatial period Λ and the acoustic wavelengths $\lambda_{x_1 m}$ and $\lambda_{x_1 \mu}$ along the x_1-axis appear ($\lambda_{x_1 m} = 2\pi/k_{x_1 m}$ for mode m generated by the source and $\lambda_{x_1 \mu} = 2\pi/k_{x_1 \mu}$ for modes μ created by the scattering on the corrugation). These relationships involve a phase matching, which emphasizes the interference processes (phonon relations[14–16]), namely,

$$k_{x_1 m} + k_{x_1 \mu} \pm 2\pi/\Lambda = 0, \tag{10}$$

i.e., using Eqs. (4b) and (8),

$$\frac{k_{x_1 \mu} d}{2\pi} = \pm \frac{d}{\Lambda} - \sqrt{\left(\frac{fd}{c_0}\right)^2 - \left(\frac{m}{2}\right)^2}. \tag{11}$$

Equation (11) shows therefore a strong coupling between the primary wave (wavenumber $k_{x_1 m}$) and the counterpropagating secondary wave (wavenumber $-k_{x_1 \mu}$). The intersection in the plane $[fd/c_0, k_{x_1 m} d/(2\pi)]$ of the dispersion curves (thick lines in Fig. 2) with the curves representing the phonon relation (11) (with $+d/\Lambda$, thin lines in Fig. 2 for $d/\Lambda = 5/3$) permits to predict the values of the frequencies for which there could be such a strong coupling for a given ratio d/Λ.

As an example, for $fd/c_0 \approx 0.92$, the thin line, which represents the phonon relation [Eq. (11)] for $m=1$, has an intersection with the dispersion curve of the regular-shaped guide corresponding to $\mu=0$ (labeled $m=0$ on the figure). Therefore, when the source creates mode $m=1$, a strong coupling appears with mode $\mu=0$. Moreover, as there is an intersection of this thin line with the dispersion curve of the guide for mode $m=1$ at a value of fd/c_0 close to 0.92, a strong self-coupling between mode $m=1$ created by the source and the same mode $\mu=1$ appears, perturbing this mode $m=1$. For a periodic sawtooth profile (Fig. 3), this is the situation presented in Fig. 4, showing the modulus of the normalized amplitudes calculated at the third-order perturbation expansion. It is assumed that, inside the two-dimensional waveguide bounded by two parallel plates, the only mode created by the source is mode $m=1$ and that the frequency is such that $fd/c_0 = 0.92$ with $d/\Lambda = 5/3$; thus, the upper modes ($\mu \geq 2$) are evanescent and the fundamental plane mode ($\mu=0$) is the only propagative mode created by coupling due to the corrugation. Figure 4(a) shows that this mode $\mu=0$ created by the scattering on the corrugation has a much greater amplitude than the evanescent coupled modes $\mu=2$ and $\mu=3$ [Figs. 4(c) and 4(d)].

The amplitude of mode $m=1$ [Fig. 4(b)] decreases when the abscissa of the observation point $(k_0 x_1)$ increases. This decrease has an approximate exponential shape, with an attenuation factor equal to approximately 10^{-3} mm^{-1} for the fictitious fluid (see Table I). The order of magnitude is the same as those obtained experimentally and theoretically in Ref. 13 (see Secs. II C and IV B and Table III).

Focusing now on the propagation upstream and downstream the roughness, the corrugation starts at the "input" abscissa x_i such as $k_0 x_i \approx 23$, and length ℓ of the corrugation, such as $k_0 \ell = 36.3$, which corresponds to $N=11$ teeth (see Table I for dimensional quantities) and to $\ell \approx 5.7\ \lambda$ for the

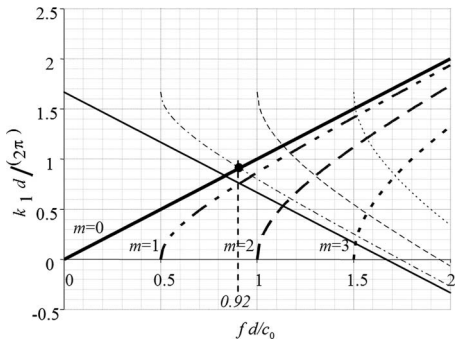

FIG. 2. Dispersion curves (thick lines) of the guide with smooth interfaces $(k_{x_1} d/(2\pi) = \sqrt{(fd/c_0)^2 - (m/2)^2})$ and curves (thin lines) corresponding to the phonon relation (11) $(k_{x_1} d/(2\pi) = d/\Lambda - \sqrt{(fd/c_0)^2 - (m/2)^2})$. Solid lines: mode $m=0$, dash-dots lines: mode $m=1$, dashed lines: $m=2$, dotted lines: $m=3$.

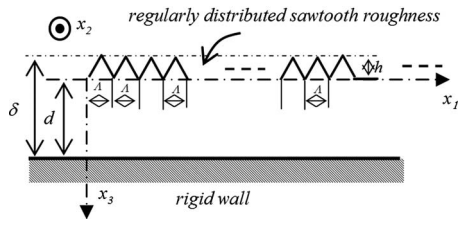

FIG. 3. Fluid plate between two rigid walls: the smooth plane wall and the wall having regularly distributed corrugations (sawtooth profile).

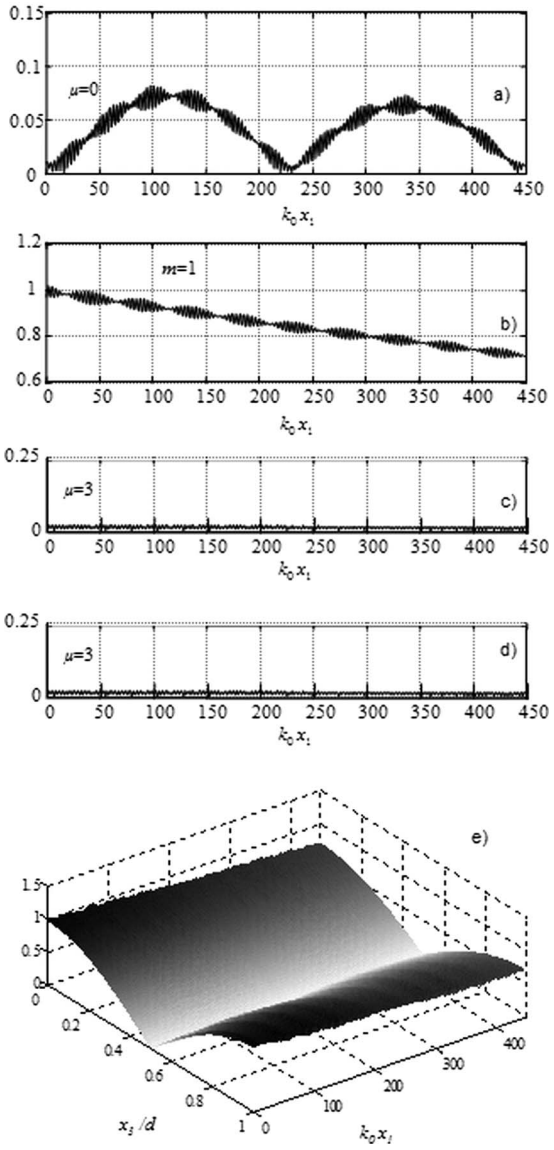

FIG. 4. Modulus of the normalized amplitude of the pressure variation (third order) for the sawtooth profile (see Fig. 3). (a) $\hat{A}^{[3]}_{\mu=0}(x_1)/A^0_m$ for mode $\mu=0$, (b) $\hat{A}^{[3]}_{m=1}(x_1)/A^0_m$ for mode $m=1$ (the only mode generated by the source), (c) $\hat{A}^{[3]}_{\mu=2}(x_1)/A^0_m$ for the evanescent mode $\mu=2$, (d) $\hat{A}^{[3]}_{\mu=3}(x_1)/A^0_m$ for the evanescent mode $\mu=3$, and (e) $|\hat{P}^{[3]}(x_1)/A^0_m|$ of the total pressure variation, when $fd/c_0=0.92$ and $d/\Lambda=5/3$. The length ℓ of the corrugation at $x_3=0$ is such that $k_0\ell=450$, which corresponds to $N=130$ teeth (see Table I for dimensional quantities) and to $\ell\approx71.5\lambda$ for the fictitious glass fluid indicated in Table I. The heights of the teeth are such that $h/d=0.005$; the interface $x_3=d$ is smooth (see Fig. 3).

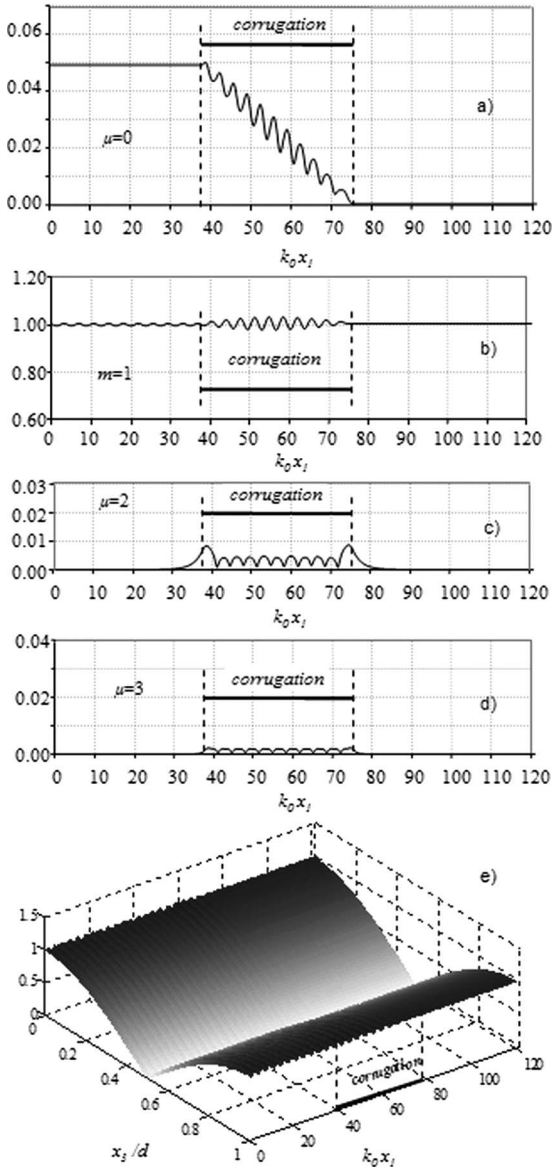

FIG. 5. Modulus of the normalized amplitude of the pressure variation (third order) for the sawtooth profile (see Fig. 3). (a) $\hat{A}^{[3]}_{\mu=0}(x_1)/A^0_m$ for mode $\mu=0$, (b) $\hat{A}^{[3]}_{m=1}(x_1)/A^0_m$ for mode $m=1$ (the only mode generated by the source), (c) $\hat{A}^{[3]}_{\mu=2}(x_1)/A^0_m$ for the evanescent mode $\mu=2$, (d) $\hat{A}^{[3]}_{\mu=3}(x_1)/A^0_m$ for the evanescent mode $\mu=3$, and (e) the total pressure variation $|\hat{P}^{[3]}\times(x_1)/A^0_m|$, when $fd/c_0=0.91$ and $d/\Lambda=5/3$. The coordinates of the ends of the corrugation are x_i and $(x_i+\ell)$ with $k_0x_i=37.7$; the length ℓ of the corrugation at $x_3=0$ being such that $k_0\ell=37.7$, which corresponds to $N=11$ crenels (see Table I for dimensional quantities) and to $\ell\approx6\lambda$ for the fictitious glass fluid indicated in Table I. The heights of the teeth are such that $h/d=0.005$; the interface $x_3=d$ is smooth (see Fig. 3).

fluidlike media indicated in Table I. The heights of the teeth or of the crenels are such as $h/d=0.005$. The modulus of the normalized amplitudes of the modes considered and the corresponding total acoustic pressure, as functions of the observation point, are given in Fig. 5. The backward propagation, created by the backscattering on corrugation, is obviously upstream the corrugation ($x_1<x_i$). Downstream the corrugation, the mode created by the source decreases when the abscissa of the observation point increases.

IV. FINITE ELEMENT METHOD: COMPARISON WITH THE INTERMODAL APPROACH

The ATILA finite element code has been used to validate the analytical results presented before.[19] The plate is divided into elements and connected by nodes. In the rough profile region, the teeth are assumed to be of infinite length and uniform in the perpendicular direction to Fig. 6 so that a bidimensional mesh is sufficient, thanks to a plane strain condition. Isoparametric elements are used, with a quadratic interpolation along the elements sides. The fluid plate considered (Table I) is divided into three domains (Fig. 6): the central domain containing eleven identical teeth (the grating) and the two domains having smooth surfaces downstream and upstream the grating. A harmonic displacement source excitation ($f=1.06$ MHz, i.e., $fd/c_0=0.91$) is set at the en-

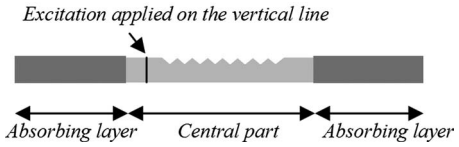

FIG. 6. Fluid plate between two rigid walls used for the FEM: the wall being plane and the wall having regularly distributed corrugations (sawtooth profile with $N=11$ teeth, spatial period $\Lambda=0.003$ m, and depth of the teeth $h=25$ μm). In order to minimize the reflection effect at the ends of the plate, absorbing layers are introduced upstream and downstream the corrugation. The harmonic excitation (mode $m=1$) is applied on the vertical line at the entrance of the corrugation.

trance of the rough domain, and absorbing layers are assumed to introduce losses outside the corrugated domain in order to minimize the parasitic reflections at the ends of the mesh. The calculation gives the pressure at each node of the mesh in the fluid plate at a given frequency.

In order to observe, at a value of fd/c_0 close to 0.92, the coupling between mode $m=1$ (assumed to be the only one created by the source) and mode $\mu=0$ created by coupling only, the acoustic pressure is analyzed in the median plane of the plate because, without teeth, it is equal to zero when mode $m=1$ propagates. The modulus of the normalized pressure, associated with the coupled mode $\mu=0$ as a function of abscissa x, is shown in Fig. 7 (thick solid line). This FEM result can be compared to the analytical one (Fig. 5(a) or thin solid line on Fig. 7). Note that the oscillations of the pressure in domain $x<0.033$ m (upstream the grating) are due to a weak reflection at the left end of the plate; they can be numerically cancelled using an appropriate method (perfectly matched absorbing layer or other methods). The backward mode $\mu=0$ results from the conversion of mode $m=0$ on each tooth; the oscillations of the curve appear to be deeply correlated with the length of the teeth of the corrugation. The amplitude of the wave downstream the corrugation is nearly equal to zero in the situation considered, as it has already been mentioned in the analytical results.

The numerically estimated value of the acoustic level (mode $\mu=0$, thick solid line of Fig. 7) in the region of the plate upstream the roughness, for frequency $f=1.06$ MHz, differs slightly from the analytical one (thin solid line of Fig. 7), with a relative error approximately equal to 25%. However, attention must be paid to the fact that the discrepancies between these results are very dependent on the frequency; changing the frequency of 3% from the value 1.06 MHz (Fig. 7, dotted line) does not change significantly the results obtained numerically. Thus, given the very small surface perturbation (the depth of the corrugation being only 0.5% of both the thickness of the plate and the wavelength, and the absolute value of the slope being lower than 2×10^{-2}), there is a quite close agreement between these analytical and numerical results, thereby supporting the fact that the analytical modeling would be accurate in the situation considered (fluid plate).

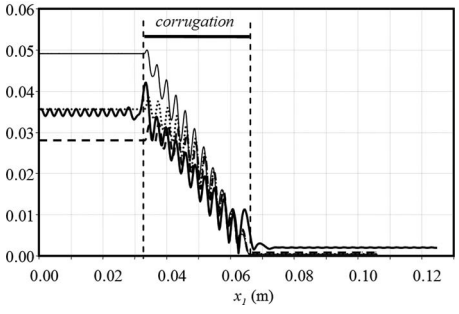

FIG. 7. Modulus of the normalized amplitude $\hat{A}^{[3]}_{\mu=0}(x_1)/A^0_m$ for mode $\mu=0$ of the pressure variation for the sawtooth profile shown in Fig. 6. Thick solid line: result obtained from ATILA finite element code when $fd/c_0=0.91$ (i.e., $f=1.06$ MHz). Thin solid line, dotted line, dashed line: results obtained from the analytical intermodal shape profile model at the third order, respectively, when $fd/c_0=0.91$ (i.e., $f=1.06$ MHz), $fd/c_0=0.936$ (i.e., $f=1.09$ MHz), and $fd/c_0=0.94$ (i.e., $f=1.1$ MHz).

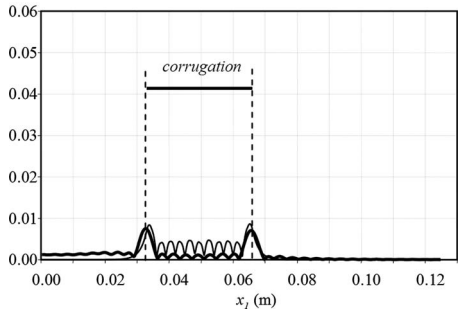

FIG. 8. Modulus of the normalized amplitude of the evanescent modes of the pressure variation for the sawtooth profile shown in Fig. 6 when $fd/c_0=0.91$ (i.e., $f=1.06$ MHz). Thick solid line: result obtained from ATILA finite element code, thin solid line: result obtained from the analytical intermodal shape profile model at the third order for the evanescent mode $\mu=2$.

At the input and at the output of the corrugated region, the amplitude of the acoustic pressure (Fig. 8, thick solid line) of all the evanescent modes increases slightly on the first and last teeth; the same kind of result has been obtained analytically for the amplitude of the evanescent mode $\mu=2$ [Fig. 5(c) or thin solid line in Fig. 8]. The amplitude value of the evanescent modes, obtained numerically (Fig. 8, thick solid line), is as expected close to the analytical value of the amplitude of the evanescent mode $\mu=2$ [Fig. 5(c) or thin solid line in Fig. 8].

V. CONCLUSION

Both analytical and numerical (FEM) methods have been used for describing the effects of a surface roughness on the waves propagating in ideal rough plates (fluid plates), with a view of characterizing bounded roughened surfaces before applying the adhesive joint. The analysis leads to (i) a physical interpretation of the phenomena by describing the mode coupling for a fluid plate using the so-called intermodal shape profile model and (ii) a validation of these latter results using a purely numerical method (FEM).

Results obtained on periodically corrugated surfaces (fluid plate and intermodal shape profile model) serve as preliminary results for randomly rough surfaces in providing physical interpretation of the phenomena observed. Notably, for the monomode shape profile model, the theoretical attenuation factor of the main Lamb mode considered, associated with a regularly distributed sawtooth roughness, is close to the result found experimentally [Part I (Ref. 13)]. Moreover, both the numerical and the analytical shapes of the

coupled modes (created by energy transfer from the main mode by coupling on the roughness), as function of the length of the roughness, are in good agreement.

Further refinements would require more advanced theoretical investigations, which imply modeling the modal coupling in rough solid plates (accounting for longitudinal and transversal waves), leading presumably to consistent results with the precision needed for characterizing the noncontact surface roughness from the measurements using ultrasonic techniques.

ACKNOWLEDGMENTS

Support from the CNRS through the research group (No. GDR-2501) was gratefully acknowledged. The authors are grateful to the reviewer for his constructive suggestion to separate the earlier version of this paper in two parts.

[1]C. C. Guyott, P. Cawley, and R. D. Adam, J. Adhes. **20**, 129 (1986).
[2]S. Banerjee and T. Kundu, J. Acoust. Soc. Am. **119**, 2006 (2006).
[3]T. Kundu, S. Banerjee, and K. V. Jata, J. Acoust. Soc. Am. **120**, 1217 (2006).
[4]S. Banerjee and T. Kundu, Int. J. Solids Struct. **43**, 6551 (2006).
[5]J. M. Claeys, O. Leroy, A. Jungman, and L. Adler, J. Appl. Phys. **54**, 5657 (1983).
[6]A. Jungman, L. Adler, J. D. Achenbach, and R. Roberts, J. Acoust. Soc. Am. **74**, 1025 (1983).
[7]B. I. Boyanov and V. L. Strashilov, IEEE Trans. Ultrason. Ferroelectr. Freq. Control **39**, 119 (1992).
[8]M. A. Hawwa, J. Acoust. Soc. Am. **102**, 137 (1997).
[9]D. H. Berman, J. Acoust. Soc. Am. **96**, 417 (1994).
[10]O. I. Lobkis and D. E. Chimenti, J. Acoust. Soc. Am. **102**, 143 (1997).
[11]K. Mampaert and O. Leroy, J. Acoust. Soc. Am. **83**, 1390 (1988).
[12]W. Lauriks, L. Kelders, and J. F. Allard, Ultrasonics **36**, 865 (1998).
[13]C. Potel, D. Leduc, B. Morvan, C. Depollier, A.-C. Hladky-Hennion, J. L. Izbicki, P. Pareige, and M. Bruneau, J. Appl. Phys. **104**, 074908 (2008).
[14]C. Potel and M. Bruneau, J. Sound Vib. **313**, 738 (2008).
[15]B. Morvan, A.-C. Hladky-Hennion, D. Leduc, and J. L. Izbicki, J. Appl. Phys. **101**, 114906 (2007).
[16]D. Leduc, A.-C. Hladky, B. Morvan, J.-L. Izbicki, and P. Pareige, J. Acoust. Soc. Am. **118**, 2234 (2005).
[17]D. Leduc, B. Morvan, P. Pareige, and J. L. Izbicki, NDT & E Int. **37**, 207 (2004).
[18]M. Bruneau and T. Scelo, *Fundamentals of Acoustics* (ISTE, United Kingdom, 2006).
[19]ATILA Finite Element Code for Piezoelectric and Magnetostrictive Transducer Modeling, Version 5.2.1, User's Manual ISEN, Acoustics Laboratory, Lille, France, 2002.